

Vortex lines or sheets – what is formed in dynamic drives?

V. B. Eltsov^{*,†}, R. Blaauwgeers^{*,‡}, N. B. Kopnin^{*,§}, M. Krusius^{*}, J. J. Ruohio^{*}, R. Schanen^{*,||},
and E. V. Thuneberg^{*,§§}

^{*}Low Temperature Laboratory, Helsinki University of Technology, P.O.Box 2200, FIN-02015 HUT, Finland

[†]Kapitza Institute for Physical Problems, Kosygina 2, 117334 Moscow, Russia

[‡]Kamerlingh Onnes Laboratory, Leiden University, P.O.Box 9504, 2300 RA Leiden, The Netherlands

[§]Landau Institute for Theoretical Physics, Kosygina 2, 117334 Moscow, Russia

^{||}Department of Physics, Royal Holloway University of London, Egham, Surrey, TW20 0EX, UK

^{§§} Department of Physical Sciences, P.O. Box 3000, 90014 University of Oulu, Finland

(November 3, 2018)

In isotropic macroscopic quantum systems vortex lines can be formed while in anisotropic systems also vortex sheets are possible. Based on measurements of superfluid ³He-A, we present the principles which select between these two competing forms of quantized vorticity: sheets displace lines if the frequency of the external field exceeds a critical limit. The resulting topologically stable state consists of multiple vortex sheets and has much faster dynamics than the state with vortex lines.

The state of superfluid ⁴He in rotation was originally explained by Onsager [1] and Landau and Lifshitz [2] by concentrating the required velocity circulation into co-axial sheets which, when viewed on large scales, give rise to solid-body-like rotation. Later, Feynman [3] showed that sheets are not stable in an isotropic superfluid and that quantized vortex lines are formed instead. The same explanation was provided by Abrikosov [4] for type II superconductors in a magnetic field.

Recently, however, the vortex sheet has staged a come back: It was theoretically suggested for unconventional superconductors [5] and experimentally verified in the anisotropic p-wave superfluid ³He-A [6]. The sheets are formed from a topologically stable domain-wall-like planar defect into which the vorticity is confined. Since these quantum systems also support vortex lines, the controversy remains: What determines the formation of lines or sheets, or alternatively, what is the difference in the macroscopic physical properties of the system when there are lines or sheets? This question is not limited to superconductors or ³He-A, but is of importance for defect formation in general, possibly in the early universe, in neutron stars, Bose-Einstein condensates, etc. – wherever non-trivial symmetry breaking into a multi-component order-parameter field may occur.

The answer whether lines or sheets are formed depends, according to our measurements of ³He-A, on the applied field: If its frequency and amplitude exceed the appropriate critical limits, sheets appear and displace lines, as shown schematically in Fig. 1. The measured phase diagram is supported by our analysis of the dynamic properties of vortex sheets, and is further confirmed by numerical simulations. The transition from lines to sheets is driven by the much faster dynamics of states with multiple vortex sheets. The roots of this phenomenon share common features with self organization and pattern formation in classical systems.

Vortex lines vs sheets.– Superconductors respond to

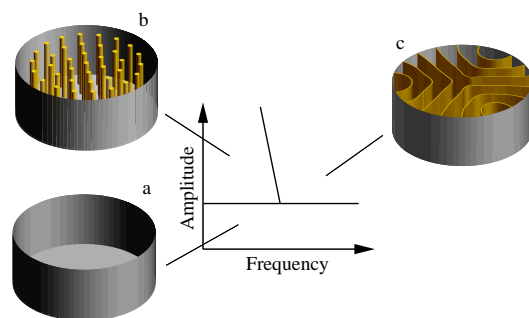


FIG. 1. The different topologically distinct states of rotating ³He-A depend on the amplitude and frequency of the drive: (a) The vortex-free Meissner state exists below a critical value of the amplitude. (b) The state with quantized vortex lines is created when the drive increases sufficiently slowly. (c) Vortex sheets are created at higher frequencies. The critical values depend on the global order-parameter texture and display large metastability.

a magnetic field by producing screening currents. Similarly, a superfluid attempts to corotate at the container's angular velocity Ω . The two motions resemble each other and usually take the form of quantized vortex lines so that the superfluid vorticity $\nabla \times \mathbf{v}_s$ is non-zero only within vortex cores, having on average the solid-body value 2Ω . In a state with sheets the irrotational superflow is channelled parallel to a sheet, while \mathbf{v}_s jumps across the sheet leaving the non-zero vorticity within the sheet. The distance between the sheets is $b = (3\sigma/\rho_s\Omega^2)^{1/3}$, where σ is the surface tension of the sheet and ρ_s the superfluid density [2]. In equilibrium, vortex lines in ³He-A have a lower energy than vortex sheets [7].

The stability of the vortex sheet rests on the existence of a two-fold degeneracy of the ground state, so that a topologically stable domain wall can exist. In ³He-A, it separates energetically equivalent states with parallel

and antiparallel orientations of the orbital $\hat{\mathbf{l}}$ and spin $\hat{\mathbf{d}}$ anisotropy directions. In superconductors with broken time-reversal symmetry the degeneracy could arise from the locking of $\hat{\mathbf{l}}$ to the crystal-field anisotropy [5]. The vorticity in the domain wall is quantized [6]; it is distributed along the wall with a period $p = n\kappa/(2\Omega b)$. Here κ is the circulation quantum and n the topological charge which depends on the structure of the vorticity. For the vortex sheet in $^3\text{He-A}$ $n = 1$ while separate vortex lines are generally doubly quantized ($n = 2$) [8].

The large-scale structure of the vortex sheet may take topologically distinct configurations with different numbers M of separated sheets. The minimum is one continuous sheet ($M = 1$) in the form of a double spiral centered around the container axis (see bottom-right inset in Fig. 3); this is the lowest energy state of a vortex sheet at constant Ω . This configuration is closest to the concentric vortex sheets originally envisioned by Onsager [1] and by Landau and Lifshitz [2]. The other extreme is the maximum number of sheets, $M_{\text{max}} = \pi R/b$, which corresponds to one connection with the lateral sample boundary per each inter-layer distance b along the perimeter of the sample ($M_{\text{max}} \approx 20$ at $\Omega = 1$ rad/s). In the absence of pinning, like in $^3\text{He-A}$, the sheets fold to fill the sample evenly since a uniform distribution of vorticity is energetically preferred. Mutual repulsion between the sheets and the boundary conditions force the sheets to be oriented perpendicular to the boundary. This promotes their radial orientation, as depicted in Fig. 1 (c).

Dynamics of lines and sheets.— A time-dependent rotation drive $\Omega(t)$ exerts a force on the circulation quanta which is mostly radial in solid-body-like rotation. The vorticity averaged over the sample, $\Omega_v = \langle |\nabla \times \mathbf{v}_s| \rangle / 2$, obeys [9]

$$d\Omega_v/dt + 2\alpha\Omega_v(\Omega_v - \Omega) = 0, \quad (1)$$

where α is the mobility in the radial direction determined by the friction from the normal excitations. Owing to the strongly anisotropic order-parameter orientations in the sheet, the mobility of vorticity in the sheet is also anisotropic. It is determined by the spatial inhomogeneity of the orbital anisotropy vector $\hat{\mathbf{l}}$ [10]:

$$\alpha_i^{-1} = \alpha_0^{-1} \int d^2r \left(\nabla_i \hat{\mathbf{l}} \right)^2. \quad (2)$$

Here i refers to the directions along \parallel or perpendicular \perp to the sheet, and $\alpha_0 = \rho_n \rho_s \kappa / (2\rho\mu)$ is related to the Cross-Anderson orbital viscosity μ [11]. We neglect an order-of-one anisotropy of ρ_s . One obtains $\alpha_{\parallel} \sim \alpha_0(p/s)$ and $\alpha_{\perp} \sim \alpha_0(s/p)$, where $s \approx 40 \mu\text{m}$ is the thickness of the sheet. The mobility of separate vortex lines is $\alpha_v \sim \alpha_0$, since the dimensions of the vortex core are $\sim s$ in all directions. Thus the mobility along the sheet α_{\parallel} is the highest: $\alpha_{\parallel} > \alpha_v > \alpha_{\perp}$. At $\Omega = 1$ rad/s one has $\alpha_{\parallel} : \alpha_v : \alpha_{\perp} \sim 4 : 1 : 1/4$. Since it is the radial mobility

that matters in Eq. (1), radial orientation of the sheets improves their dynamic response.

For the dynamics also the creation and annihilation of vorticity is crucial. The circulation quanta are created at a critical velocity which depends on the order-parameter texture [12]. For vortex sheets, vorticity is created at the connection lines of the sheets with the boundary where the order-parameter field is already distorted and the critical velocity is reduced compared to vortex lines [6]. Thus multiple sheets with their $2M$ connection lines provide a large number of effective nucleation sites. These inject new vorticity much more efficiently than the competing alternative, one nucleation center of vortex lines close to the lateral sample boundary [8].

To conclude, the different rates of dynamic response, which control relaxation towards the instantaneous equilibrium, are expected to govern the transition between lines and sheets: A high-frequency drive at sufficient amplitude should replace all other forms of vorticity with radially oriented multiple vortex sheets. The transition can occur in the following way: At high frequency the order-parameter texture around a nucleation center, where vortex lines are periodically nucleated and annihilated, may become locally unstable and the beginning of a domain-wall defect may be created. When existing vortex lines have been annihilated during a subsequent decrease in the drive, the new vorticity may now re-enter during the next increase in the drive via the domain-wall defect, where the critical velocity is reduced and the mobility is enhanced. A single sheet is unstable in an oscillating drive and, as discussed later, this leads to the formation of a state with multiple sheets. A configuration with a given number of sheets is topologically stable and will persist as a metastable state if the time-dependent component in the drive is switched off and Ω is kept constant.

Measurement of topological transitions.— Our measurements on $^3\text{He-A}$ have been performed on a cylindrical sample with a radius $R = 2$ mm in an axial magnetic field of 9.6 mT, pressure 33 bar, and temperature 1.7 mK, by rotating the entire refrigerator. NMR spectroscopy is used to identify the various order-parameter topologies. Vortex lines or sheets produce characteristic NMR satellite peaks, while in the vortex-free state there is no satellite. Although the satellites may overlap (Fig. 2, insert), they have different dependencies on Ω which distinguishes between lines and sheets [6]. The rotation drive is thus used both for generating transitions between the states and as a detection tool.

The lower part of Fig. 2 illustrates transitions between the three rotating states of Fig. 1 as a function of time t when the drive $\Omega(t) = \Omega_1 \sin \omega t$ is switched on. The starting state is vortex free with no satellite. Vortex lines begin to form when Ω reaches the critical value $\Omega_c \approx 0.24$ rad/s during the first half period. Here the height of the satellite is proportional to the *total number* of vortex lines. The characteristic features are two plateaus during

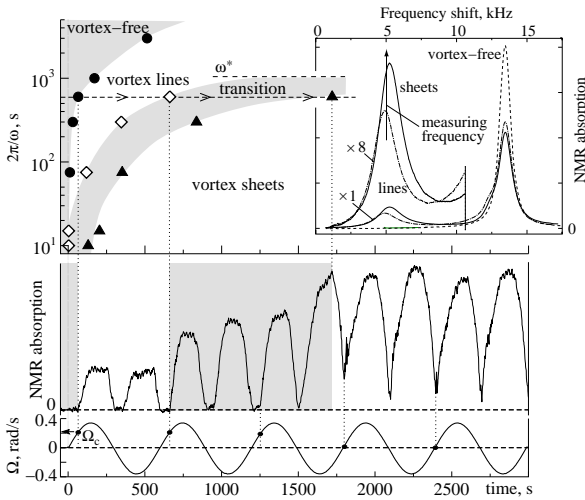


FIG. 2. (Top) Sequence of transitions (vortex-free \rightarrow vortex lines \rightarrow vortex sheets), when the drive $\Omega(t) = \Omega_1 \sin \omega t$ (with $\Omega_1 = 0.35$ rad/s) is switched on: (●) first appearance of lines, (◇) transition to sheets starts, (▲) transition to sheets is completed. The vertical axis is the period $2\pi/\omega$ of the drive while the horizontal axis is the common time axis (t) with the bottom panel. (Bottom) Height of the vorticity satellites as a function of time after switching on the drive $\Omega(t)$, with $2\pi/\omega = 600$ s which corresponds to the path along the dashed arrow in the top panel. The signal is recorded at the NMR frequency shown in the insert. The drive $\Omega(t)$ is plotted below the satellite signal. (Insert) NMR absorption spectra of the rotating states with lines and sheets at $\Omega = 2.4$ rad/s and of the vortex-free state ($\Omega < \Omega_c$).

one half cycle: the first at zero height when $|\Omega|$ increases from 0 to Ω_c , and the second at maximum absorption when $|\Omega|$ decreases from Ω_1 to roughly $\Omega_1 - \Omega_c$. The plateaus correspond to zero and to maximum number of vortex lines, respectively.

After one full period the conversion to vortex sheets starts. The response gradually changes and acquires features characteristic to the vortex sheet: The satellite height grows larger and the plateaus disappear. For a sheet, the signal height is proportional to its *total length*. The critical velocity is now vanishingly small which ensures the smooth growth and shrinkage of the sheets as a function of Ω . Also, the satellite height does not reach zero when Ω changes sign because the backbone of the sheet – the domain wall – does not have time to drift away and continues to contribute to the signal even in the absence of circulation at $\Omega = 0$. These features can be studied in detail, by switching off the modulation of the drive at any moment. Thereafter Ω can be kept at constant value, and the entire NMR absorption spectrum can be recorded to determine the frequency shift and height of the satellite.

The upper left panel of Fig. 2 illustrates how long it takes to complete the transitions at different ω . Note that there exists a characteristic frequency ω^* such that

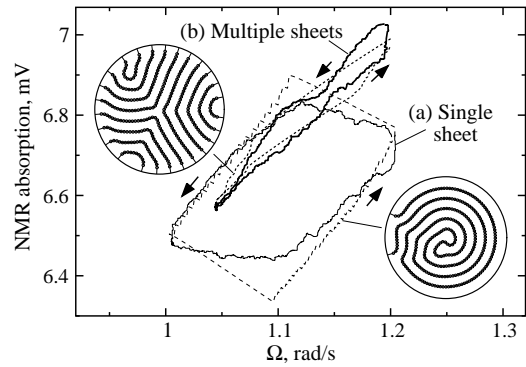


FIG. 3. Measured hysteresis loops in satellite-peak height when Ω is slowly changed (solid lines). (a) An adiabatically grown single sheet. (b) Multiple sheets created from the single sheet by subjecting it to high-frequency modulation [$\Omega(t) = (0.4 \sin \omega t + 1.2)$ rad/s, with $2\pi/\omega = 10$ s]. The broken lines represent numerical simulations for the configurations shown in the respective inserts. The only fitting parameter is the coefficient of proportionality which connects the total length of the sheets to NMR absorption.

$2\pi/\omega^* \sim 10^3$ s which separates lines and sheets in the limit $t \rightarrow \infty$: At $\omega < \omega^*$ a response in terms of lines is stable while at $\omega > \omega^*$ sheets appear. The conditions in the lower panel correspond to the case when $\omega > \omega^*$ and sheets are stable. The larger the drive frequency ω , the faster the transition to sheets starts. Finally, with $2\pi/\omega \lesssim 20$ s the transition to sheets starts directly from the vortex-free state, with no indication of a signal from vortex lines in between. With increasing drive amplitude Ω_1 the transition to sheets ω^* moves to lower frequencies and is completed faster. Thus the transition line $\omega^*(\Omega_1)$ is tilted as shown in Fig. 1.

Identification of sheet topologies.– Different vortex-sheet configurations can be studied by measuring the Ω -dependence of the NMR satellite. This can be recorded either in the adiabatically slow limit (Fig. 3) or as a dynamic response (Fig. 4). To analyze the response of a state with multiple sheets it is instructive to compare it to that of the well-known configuration with a single continuously coiled sheet. The latter provides a convenient reference which can be grown adiabatically from a single seed of domain wall, by slowly increasing Ω from zero [6].

Let us calculate the total sheet length L for a given number of sheets M and circulation quanta N . The vorticity is isolated from the lateral sample boundary by an annular vortex-free superflow and confined within a radius $R_v = \sqrt{\kappa N}/2\pi\Omega$. These central sections of the sheets amount to a total length of $\pi R_v^2/b$. At the sample boundary the $2M$ ends of the M vortex sheets cross the vortex-free region of width $d = R - R_v \ll R$. We have

$$L = \pi R_v^2/b + 2Md \approx \pi R^2/b + 2d(M - M_{\max}). \quad (3)$$

In Fig. 3, loop (a) is traced by a single sheet ($M = 1$): (i) In the lower branch of the loop which starts from

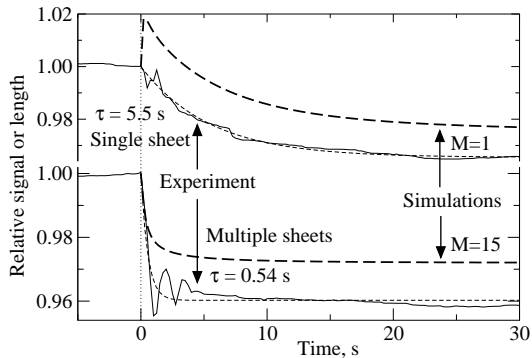


FIG. 4. Dynamic responses of two different vortex sheet configurations to a step change in rotation velocity $\Delta\Omega = -0.15$ rad/s (at $t = 0$), with $\Omega = 1.25$ rad/s initially. The satellite-peak heights (solid lines) normalized to the initial values are recorded as functions of time t . The thin broken lines show exponential fits to determine the response time τ . The thick dashed lines show the results from numerical simulations ($\sigma/\rho_s = 1.1 \cdot 10^{-8}$ cm³ s⁻², $\alpha_0 = 30$). The initial increase in the uppermost curve is the out-of-phase response of the single sheet (at $N = \text{const}$), which becomes experimentally visible only at higher drives $\Omega \gtrsim 1.8$ rad/s [13].

1.1 rad/s in increasing Ω , the counterflow velocity at the boundary is at the critical value and new vorticity is created while d is almost constant. We find from Eq. (3) that $L \approx \pi R_v^2/b \propto N\Omega^{-1/3}$, if we neglect the small term $2Md$. Since $N \propto \Omega$, the length is $L \propto \Omega^{2/3}$ and $dL/d\Omega \approx (2/3)L/\Omega > 0$, which agrees with the positive slope above 1.1 rad/s. (ii) During decreasing Ω , N first remains constant, before the annihilation threshold is reached. In this branch $L \propto \Omega^{-1/3}$ so that $dL/d\Omega \approx -(1/3)L/\Omega < 0$. This again agrees with the almost twice smaller negative slope when Ω first decreases below 1.2 rad/s. The out-of-phase response (L increases while the drive Ω decreases) is the most distinct characteristic of the single-sheet response at constant number of circulation quanta ($\Omega_1 \leq \Omega_c$) [13]. (iii) At the annihilation threshold (branch with $\Omega \lesssim 1.1$ rad/s, $d\Omega/dt < 0$), vorticity is expelled, $d \approx \text{const}$, and again $dL/d\Omega \approx (2/3)L/\Omega > 0$. (iv) Finally, the negative slope of $dL/d\Omega$ is resumed in the last leg of the loop where Ω is increased back towards the critical velocity.

In contrast multiple sheets, Fig. 3 loop (b), with $M \approx M_{\text{max}}$, have always $L \propto b^{-1}$, as seen from Eq. (3), and $dL/d\Omega \approx (2/3)L/\Omega > 0$ in agreement with the measured narrow hysteresis loop. The in-phase response dominates the output from states with multiple sheets. The prominent difference in the responses of the two sheet configurations in Fig. 3 has thus a simple explanation in terms of one adjustable variable M .

Dynamic response.— To illustrate the faster dynamics of a state with multiple sheets, Fig. 4 provides a comparison to the single sheet. The responses are recorded to a step-like change in the rotation drive. The vortic-

ity relaxes with time constant $\tau = (2\alpha\Omega)^{-1}$ which is an order of magnitude smaller for the multiple-sheet state than for the single sheet.

Simulation.— These and other measurements can be compared to numerical simulation, by extending the model in Ref. [14] to dynamical processes with an anisotropic mobility [15]. In comparing the responses of different configurations to slow changes in Ω (Fig. 3), it appears that the most important factor is the number of sheets, whereas the detailed arrangement of the sheets is less influential. Our dynamical simulations confirm that in an oscillating drive, a single sheet transforms into multiple sheets: When Ω increases rapidly azimuthal sections of the sheet become unstable. When the number of circulation quanta grows, an azimuthal outer sheet becomes overfilled as the quanta have no time to move inside the sheet. This section then becomes corrugated and a bulge is formed, to redistribute the vorticity more evenly. During the subsequent decrease of Ω the vorticity expands and the bulge may touch the sample boundary. This produces two new connections and improves the radial alignment of the sheets. Ultimately, the faster motion of vorticity in such sheets suppresses the formation of new bulges when M has grown to $(0.6 \div 0.8)M_{\text{max}}$. In Fig. 4 the step response of such a dynamically created sheet configuration is compared to that of the single sheet from which it was created. In both cases the measured curves are in reasonable agreement with the calculations.

Conclusion.— Superfluid ³He-A provides the first example of a quantum system where the temporal properties of the external field determine in what form of quantized vorticity the response occurs. As a function of frequency, a topological transition takes place from linear to planar order-parameter configurations. Among all possible states of vorticity in ³He-A, a state with radially oriented multiple vortex sheets is established that provides the fastest dynamic response at high frequencies. Many of the features, which make this phenomenon possible are also present in other systems with a multi-component order parameter, and thus this could be a generic property of quantum systems with intrinsic anisotropy.

We thank E. Sonin and G. Volovik for instructive discussions. This work was funded by the EU-IHP program and by the Russian Foundation for Basic Research.

-
- [1] L. Onsager; see R.J. Donnelly, *Quantized vortices in He-II* (Cambridge Univ. Press, Cambridge, 1991), p. 48.
 - [2] L.D. Landau and E.M. Lifshitz, *Doklady Akademii Nauk SSSR* **100**, 669 (1955).
 - [3] R.P. Feynman, *Prog. Low Temp. Phys.*, C.G. Gorter, ed., (North-Holland, Amsterdam, 1955) Vol. 1, p. 17.
 - [4] A.A. Abrikosov, *Zh. Eksp. Teor. Fiz.* **32**, 1442 (1957) [*Sov. Phys. JETP* **5**, 1174 (1957)].
 - [5] M. Sigrist, K. Ueda, *Rev. Mod. Phys.* **63**, 239 (1991); M. Sigrist, *Physica B* **280**, 154 (2000).

- [6] Ü. Parts *et al.* Phys. Rev. Lett. **72**, 3839 (1994); Physica B **210**, 311 (1995).
- [7] Ü. Parts *et al.*, Phys. Rev. Lett. **75**, 3320 (1995); J. Karimäki, E. Thuneberg, Phys. Rev. B **60**, 15290 (1999).
- [8] R. Blaauwgeers *et al.*, Nature **404**, 471 (2000).
- [9] E.B. Sonin, Rev. Mod. Phys. **59**, 87 (1987).
- [10] N.B. Kopnin, Zh. Eksp. Teor. Fiz. **74**, 1538 (1978) [Sov. Phys. JETP **47**, 804 (1978)].
- [11] H.E. Hall, J.R. Hook, *Prog. Low Temp. Phys.*, (Elsevier Science, Amsterdam, 1985) Vol. 9, p. 143.
- [12] V.M. Ruutu *et al.*, Phys. Rev. Lett. **79**, 5058 (1997).
- [13] V.B. Eltsov *et al.*, Physica B **284–288**, 254 (2000).
- [14] M.T. Heinilä, G.E. Volovik, Physica B **210**, 300 (1995); V.B. Eltsov, J. Low Temp. Phys. **121**, 387 (2000).
- [15] V.B. Eltsov *et al.*, to be published.